On the choice of the parameter identification procedure in quasi-dynamic testing of low-temperature solar collectors

J. M. Rodríguez-Muñoz[a,*], I. Bove[b], R. Alonso-Suárez[a,b], P. A. Galione[c]

[a] *Laboratorio de Energía Solar, Departamento de Física del Litoral, CENUR Litoral Norte, Universidad de la República*
[b] *Laboratorio de Energía Solar, Instituto de Física, Facultad de Ingeniería, Universidad de la República*
[c] *Laboratorio de Energía Solar, Instituto de Ingeniería Mecánica y Producción Industrial, Facultad de Ingeniería, Universidad de la República*

Abstract

The ISO 9806:2017 standard is widely used to characterize the thermal performance of solar collectors. It permits two test methods: Steady State Testing (SST) and Quasi-Dynamic Testing (QDT). While SST requires high stability and clear sky conditions, which limit its application, QDT offers more flexibility in sky conditions. In contrast, the QDT method adds complexity due to the handling of transient phenomena during data processing. There are two approaches to parameter identification in QDT: multilinear regression (MLR) and dynamic parameter identification (DPI). MLR, the most common tool, faces challenges with certain collector types and its results depend on the data averaging time. DPI, while more complex, has the potential to overcome MLR's shortcomings. Which of these two methods is most suitable for testing low-temperature solar collectors in a broad sense is an issue that has not yet been addressed. This work provides evidence that the DPI procedure is more convenient than the MLR procedure, especially for evacuated tube collectors with heat pipes. Specifically, it is shown that DPI produces more reliable test results and provides more accurate estimates of useful power, and it exhibits less variability with respect to data averaging time, demonstrating its improved robustness.

Keywords: Solar thermal collector, dynamic parameter identification, transient model, ISO 9806 standard.

1. Introduction

The ISO 9806:2017 [1] is the most widely used standard for characterizing the thermal performance of solar collectors. It establishes a general thermal model that can be used for a wide variety of technologies: flat plate, evacuated tube, concentrating, etc., both for water and air solar heating systems. Although there are other standards such as ASHRAE-93 [2], they have a high degree of similarity, making them essentially equivalent to each other [3]. The ISO 9806:2017 standard includes two test procedures: Steady State Testing (SST), which requires a high degree of system stability (including flow rate, inlet temperature,

*Corresp. author: J. M. Rodríguez-Muñoz, jrodrigue@fing.edu.uy

List of Symbols

$\dot{m}$	Mass flow rate, $\mathrm{kg\,s^{-1}}$.
$\dot{Q}_u$	Useful power produced by the collector, W.
$\eta_{0,b}$	collector peak efficiency referred to direct solar irradiance.
$\eta_{0,hem}$	collector peak efficiency referred to global solar irradiance.
θ	Incidence angle.
θ_L	Longitudinal angle of incidence.
θ_T	Transversal angle of incidence.
ϑ_a	Ambient air temperature, °C.
ϑ_i	Collector inlet temperature, °C.
ϑ_m	Mean temperature of heat transfer fluid, °C.
ϑ_o	Collector outlet temperature, °C.
a_1	Heat loss coefficient, $\mathrm{W/m^2K}$.
a_2	Temperature dependence of the heat loss coefficient, $\mathrm{W/m^2K^2}$.
a_5	Effective thermal capacity, $\mathrm{J/Km^2}$.
A_G	Gross area of collector, $\mathrm{m^2}$.
f_d	Diffuse fraction, G_{dt}/G_t.
G_{bt}	Direct solar irradiance on collector plane, $\mathrm{Wm^{-2}}$.
G_{dt}	Diffuse solar irradiance on collector plane, $\mathrm{Wm^{-2}}$.
G_t	Global solar irradiance on collector plane, $\mathrm{Wm^{-2}}$.
K_b	Incidence angle modifier for direct solar irradiance.
K_d	incidence angle modifier for diffuse solar irradiance.
K_{bL}	Incidence angle modifier in the longitudinal plane.
K_{bT}	Incidence angle modifier in the transversal plane.
K_{hem}	Incidence angle modifier for global solar irradiance.
q	Volumetric flow rate, $\mathrm{L\,min^{-1}}$.
u	Surrounding air speed, $\mathrm{m\,s^{-1}}$.

solar irradiance, wind speed, etc.), and Quasi-Dynamic Testing (QDT), where stability conditions are more flexible. Numerous publications have demonstrated the equivalence between these methods, using the current ISO 9806:2017 standard for flat plate collectors (FPC) [4] and evacuated tube collectors (ETC) [5], as well as the European standard EN 12975 for the same technologies, FPC [6] and ETC [7]. The latest version of this standard has become a requirements standard from now on, referring to ISO 9806. This work focuses on the QDT method, specifically for water heating systems, considering the two main solar collector technologies: flat plate and evacuated tube. Next, a brief background on the QDT methodology is provided.

1.1. State of the art

The SST methodology requires strict control of test variables, particularly solar irradiance stability. As a result, outdoor testing must adhere to strict clear-sky conditions, limiting the viability of testing in regions with variable cloud conditions. In contrast, the less common QDT methodology allows for collector operation under a variety of sky conditions - clear, partly cloudy, and completely cloudy. This flexibility makes quasi-dynamic testing more suitable for climates with variable cloudiness, resulting in shorter testing times and increased testing capacity for outdoor laboratories, as shown for temperate climate zones in Europe [7] and Latin America [8]. However, data processing for the QDT method becomes more complex due to the management of transient collector behavior and the separation modeling of direct and diffuse solar irradiance.

There are two different approaches to determining the parameters of the models in the QDT methodology [6], which differ in how they handle transient phenomena. The first method involves approximating the time derivative using finite differences and treating it as an independent variable in a regression algorithm, commonly known as multi-linear regression (MLR). The second method is to perform a dynamic simulation coupled with a non-linear regression algorithm (Dynamic Parameter Identification, DPI). While DPI offers advantages over the MLR method, its implementation is more challenging. The study by Muschaweck and Spirkl [9] represents one of the early precedents for this procedure for FPC. The thermodynamic model used in this work was later improved by Bosanac [10], becoming more similar to the current thermal model suggested by ISO 9806:2017 for this type of collector. Fischer et al. [11] demonstrated the equivalence between these two methods for four different flat plate collectors. The equivalence for evacuated tube collectors has not been addressed yet.

The MLR method is the most widely used tool due to its simplicity and has been implemented in a variety of technologies. In addition to the FPC and ETC collectors already mentioned, there are also precedents for their application to uncovered collectors [7], parabolic trough collectors [12] and Fresnel concentrators [13]. However, it has some disadvantages, which are summarized below. First, MLR results depends of averaging time used for experimental data [14]. Although a 30-second averaging time is suggested by the standard, it is well known that small averaging time duration can create difficulties in the parameter identification process. Typically, data averaging times of 5 to 10 minutes are used, producing results similar to those of the SST method. The specific data averaging time that provides the best results, closest to SST parameter values, depends on the collector technology. Second, while this methodology is widely used in the context of flat plate collectors, some difficulties have been reported when trying to extend this methodology to evacuated tube collectors with heat pipes [15]. These types of collectors have a much larger time constant compared to other technologies, and the MLR method has difficulty in accurately describing the temperature variations at the collector outlet. This makes it difficult to determine some of the characteristic parameters, especially those related to the incident angle modifier. Finally, the MLR method must limit temperature variations at the collector inlet. This is not a problem in QDT testing because the standard itself imposes a limit on the variability, but it becomes an issue in the context of in-situ testing [14].

The DPI procedure has the potential to overcome the disadvantages of the MLR method. In this regard, DPI allows the use of test data with high temporal resolution, e.g. 10 seconds, as shown in [13], as well as a 5-minute average, as shown in [10]. Therefore, this procedure appears to be more robust in handling different data averaging times. On the other hand, DPI provides greater flexibility regarding the thermodynamic model of the collector [11], allowing the use of more sophisticated models. For example, it allows the use of multi-nodal models, which have been shown to be suitable for in-situ testing and are able to handle significant variations in fluid temperature at the collector inlet [14]. Finally, it is worth noting that the combination of multi-node models and high temporal resolution test data allows a more accurate reproduction of the real collector dynamics, improving the modeling of transient phenomena and resulting in shorter test times [13].

The disadvantage of the DPI procedure is that its implementation requires the use of more complex mathematical tools. While some implementations are available for the kind of collector used in this work, they often rely on closed-code or paid programs [14], making replication difficult. Furthermore, the implementation of this method for evacuated tube collectors has not yet been reported in the literature, compromising the generality of the method, which represents another limitation of this approach.

1.2. Article's contribution

The main objective of this work is to demonstrate that the DPI procedure is the better choice for QDT testing of low-temperature solar collectors.

It is observed that critical aspects of the QDT method are significantly improved through this procedure, especially for evacuated tubes. To achieve this objective, a specific implementation of the DPI procedure for both types of collectors is presented and experimentally validated against SST results and compared to QDT-MLR results. Specifically, the test data from a Flat Plate Collector (FPC) and an Evacuated Tube Collector with Heat Pipes (ETC-HP) are considered. This work represents the first case of implementation of the DPI procedure for ETC-HP collectors. Thus, it represents a significant progress in demonstrating the generality of the DPI procedure, that is, its application to different technologies.

The advantage of the DPI procedure demonstrated in this work are the following. First, through sensitivity analysis and comparison with MLR results, it is shown that the DPI procedure has less variability in terms of data averaging time. While for the MLR method this variable (data averaging time) has to be set specifically for each type of collector, in the DPI procedure this variable can be set within a wide range without compromising the results. The ability of the DPI procedure to work with data of high temporal resolution is demonstrated, showing the superiority of this procedure over the MLR in terms of parameter uncertainty and the consequent precision of the useful power estimation. Furthermore, it is shown that DPI reduces the problems associated with the determination of the IAM in the case of ETC technology. It provides more reliable results and allows to reduce the test duration by shortening the sequences related to the IAM determination.

Finally, to address one of the major drawbacks of the DPI procedure, a free and explained computational code is provided. This not only facilitates the replication of this work, but also aims to broaden the application of the DPI procedure to test laboratories worldwide. The availability of such free and open algorithms is an important foundation for future research in the field of solar collector testing, which has not been provided in previous related work.

1.3. Article's outline

This article is organized as follows. In the following section, Section 2, we describe the thermodynamic model proposed by the ISO 9806:2017 standard for low-temperature glazed solar collectors, along with the specific DPI algorithm implemented in this work. In Section 3, we provide detailed information about the test platform, the collectors tested and the measurements performed. In Section 4, we present the results obtained using the DPI procedure and compare them with SST and QDT-MLR results, thus providing experimental validation for the proposed DPI procedure. This section also highlights the advantages of the DPI procedure over the MLR and discusses the findings. Finally, Section 5 summarizes the main conclusions.

2. Methodology

This section describes the thermodynamic model used for the QDT methodology, the test procedure, and the dynamic parameter identification algorithm introduced in this work.

2.1. Thermodynamic model and parameters

The thermodynamic model used by the quasi-dynamic method in the ISO 9806:2017 standard is quite general and applicable to different solar collector technologies. The standard provides guidelines for using the model in each case, specifying the terms that can be omitted from the general equation based on the technology of the solar collector being tested. The proposed model for low-temperature glazed collectors is shown in Eq. (1):

$$\frac{\dot{Q}_u}{A_G} = \eta_{0,b}\left[K_b\left(\theta\right)\ G_{bt} + K_d\ G_{dt}\right] - a_1\left(\vartheta_m - \vartheta_a\right) - a_2\left(\vartheta_m - \vartheta_a\right)^2 - a_5\frac{d\vartheta_m}{dt}, \tag{1}$$

where $\dot{Q}_u$ is the useful power produced by the collector (i.e. delivered to the heat transfer fluid), G_{bt} and G_{dt} are the direct and diffuse solar irradiance on the collector plane, respectively, ϑ_m is the average temperature of the fluid passing through the collector (it is calculated as the average of the inlet and outlet temperatures, assuming a linear temperature variation along the collector), ϑ_a is the ambient temperature, and the set of parameters p that characterize the thermal behavior of the collector are: $\eta_{0,b}$, K_b, K_d, a_1, a_2 and a_5. The first parameter is the optical efficiency of the collector at normal incidence referred to direct solar irradiance, a_1 and a_2 are the thermal loss factors, a_5 is the effective thermal capacity divided by the gross collector area (A_G), and K_b and K_d are the incident angle modifiers (IAM – Incident Angle Modifier) with respect to direct and diffuse solar irradiance, respectively.

All parameters are constant except the IAM associated to the direct solar irradiance, K_b, which varies with the angle of incidence, θ. For this function we use the model of [4], originally designed for flat plate collectors and then extended to evacuated tube collectors in [5]. Thus, it is a general model applicable to different technologies (uniaxial and biaxial IAM). This model involves dividing the incident angle range into smaller intervals and using a piecewise linear function within each interval. For example, with a 10° interval, the adjustable parameters would be $K_b(10°), K_b(20°), \ldots, K_b(80°)$, where $K_b(\theta_i)$ is the K_b value at angle θ_i. It is set that $K_b(0°) = 1$ and $K_b(90°) = 0$. This approach outperforms other models over a wide range of incidence angles as shown in [4].

In the case of evacuated tube collectors, K_b is a function of two angles of incidence, θ_L and θ_T, corresponding to angles projected onto two perpendicular planes. We use the simplification of [16], factorizing the IAM into two different functions: $K_b = K_{bL} \times K_{bT}$. Here, K_{bL} denotes K_b computed at $(\theta_L, 0)$, and K_{bT} denotes K_b computed at $(0, \theta_T)$. In this case, the discretization process was applied to both K_{bL} and K_{bT}.

2.2. Test procedure

In the QDT method, parameter identification involves a single test that requires the execution of at least one measurement sequence for each designated day type. Each day type corresponds to a specific measurement sequence defined by the standard. The total number of sequences required will depend on local climatic conditions and the timing of the test. Each day type should last a minimum of 3 hours and may consist of several non-consecutive sub-sequences, each lasting a minimum of 30 minutes. There are four different day types, each with specific conditions as described in the following paragraph.

Day type 1 requires running sequences where the fluid temperature is close to the ambient temperature, primarily under clear sky conditions. The angle of incidence is varied within a specified range to provide sufficient variability for the K_b function. Day Type 2 involves measurements under varying cloud cover conditions. Day Type 3 requires the collector to operate at an intermediate inlet temperature, at least two different temperatures are required, and Day Type 4 requires a high inlet temperature sequence. Both day types 3 and 4 must include clear sky measurements. Guidelines for improving the clarity of parameter identification for ETC-HP technology are outlined in [5, 15].

To ensure that the experimental data set contains sufficient variability for accurate parameter identification, the standard recommends generating the following plots: 1) $(\vartheta_m - \vartheta_a)$ as a function of G; 2) G_{bt} as a function of θ; 3) G_{dt} as a function of G; and 4) $(\vartheta_m - \vartheta_a)$ as a function of wind velocity parallel to the collector area, u. These plots should be compared to the typical plots of the standard and show a significant degree of similarity. Variability in this work is ensured in accordance with the ISO 9806:2017 standard.

Although this work focuses primarily on the QDT method, the SST method is also implemented and presented in Section 4 as a baseline and reference. The SST method is well known and described in numerous references, such as [7], and therefore its detailed explanation is omitted.

2.3. Parameter identification algorithm for QDT methodology

There are two parameter identification procedures for the QDT method [6]: (i) the finite difference approximation of the time derivative and (ii) dynamic parameter identification. In both cases, the aforementioned thermodynamic model is used and the mean squared error of the useful power serves as the objective function for minimization:

$$E_c(p) = \frac{1}{M}\sum_{i=1}^{M}\left[\dot{Q}_u(t_i) - \dot{Q}_u^*(t_i,p)\right]^2, \tag{2}$$

where $\dot{Q}_u(t_i)$ represents the useful power produced by the collector at time t_i (experimental measurement), $\dot{Q}_u^*(t_i,p)$ is the model estimate of useful power at the same time, and M is the number of measurements. Note that the mean squared error is a function of the parameters, i.e., $E_c = E_c(p)$. The goal of the regression algorithm is to find the parameter set $\hat{p}$ that minimizes the function $E_c(p)$.

Regarding the regression algorithm, in this study the Two-Metric Projection method has been implemented for both parameter identification procedures [17]. This algorithm is iterative, non-linear and constrained, and its versatility is highlighted, being suitable for different collector technologies. Furthermore, its constraints ensure convergence to physically plausible values. To reduce the algorithm's susceptibility to local minima, the procedure is iterated with 10 different randomly generated starting points, and the solution with the smallest mean square error is selected. Parameter uncertainties are estimated using a linearization approach [13]. Detailed information on this algorithm can be found in [5].

The parameter identification procedures, MLR and DPI, differ in how they estimate $\dot{Q}_u^*$. In particular, the procedures differ in their approach to transient effects, which is discussed in detail in the following subsections. In both cases, averages of the variables involved should be taken every certain time interval.

2.3.1. Approximation of derivative by finite difference (MLR)

The essence of this method is a finite difference approximation of the time derivative of the mean temperature of the fluid, as follows:

$$\frac{d\vartheta_m}{dt} \cong \frac{\vartheta_m(t+\Delta t) - \vartheta_m(t)}{\Delta t}. \tag{3}$$

where Δt is the data averaging time, $\vartheta_m(t)$ and $\vartheta_m(t+\Delta t)$ are, respectively, the experimental average temperature of the fluid at the beginning and at the end of the time interval Δt. The estimated useful power produced by the collector, $\dot{Q}_u^*$, is estimated using Eq. (1) in combination with Eq. (3). Subsequently, the term $d\vartheta_m/dt$ serves as an additional independent variable in the regression algorithm, along with the other measured variables on the right side of Eq. (1): ϑ_i, ϑ_a, θ, G_b, and G_d, averaged over Δt.

Note that in this procedure, the regression algorithm can be either linear or non-linear, depending on the collector technology. In the case of flat plate collectors, the thermodynamic model can be expressed linearly in terms of the parameters. Thus, the regression problems can be reduced to a simple Multi-Linear Regression (MLR) algorithm. Since the first implementations of this procedure were applied to flat plate collectors [18], this procedure is commonly known as MLR. However, as mentioned before, for the generality of this work, a non-linear algorithm has been chosen.

This procedure is applicable to different collector technologies and is widely used as mentioned above, mainly due to its simplicity of implementation. In particular, we highlight the previous work of [5], a study that provides a computational program for parameter identification using the QDT methodology through the MLR procedure. This program is intended for general use with low temperature glazed solar collectors.

2.3.2. Dynamic parameter identification (DPI)

This procedure differs from the previous one in that it requires a dynamic simulation of the collector. Specifically, the estimation of the mean fluid temperature, ϑ_m^*, is obtained by solving the differential equation provided by Eq. (1) based on the input variables and a set of characteristic parameters p. Once this equation is solved, $\dot{Q}_u^*$ is estimated as follows,

$$\dot{Q}_u^* = 2\ \dot{m}\ c_p\ \left(\vartheta_m^* - \vartheta_i\right), \tag{4}$$

where $\dot{m}$ and ϑ_i correspond to the experimental measurements of mass flow rate and fluid temperature at the collector inlet, respectively. To distinguish experimental measurements from estimates, an asterisk notation is used. Variables with an asterisk (e.g., $\dot{Q}_u^*$) represent estimates, while those without it correspond to experimental measurements.

The input variables correspond to measurements of the relevant variables in the collector modeling: ϑ_a, θ, G_b, and G_d, which are added to the previously mentioned ϑ_i and $\dot{m}$. These input variables are time-dependent functions (averaged over Δt), but remain constant during each iteration of the regression algorithm, while the characteristic parameters of the collector vary in each iteration.

In this work, the differential equation is solved numerically with the procedure that is explained below. To do this, Eq. (1) is first combined with Eq. (4) and conveniently rewritten as follows:

$$\frac{d\vartheta_m^*}{dt} = \frac{A_G}{a_5}\left(\eta_{0,b}\left[K_b\left(\theta\right)\ G_{bt} + K_d\ G_{dt}\right] - a_1\left(\vartheta_m^* - \vartheta_a\right) - a_2\left(\vartheta_m^* - \vartheta_a\right)^2 - \frac{2\dot{m}c_p\left(\vartheta_m^* - \vartheta_i\right)}{A_G}\right). \tag{5}$$

Then, the value of ϑ_m^* at a generic time t_i, i.e., $\vartheta_m^*(t_i)$, is determined by integrating Eq. (5) between the times t_{i-1} and t_i, assuming the value of ϑ_m^* at the initial time t_0 is known. This integral is performed using the trapezoidal rule. For simplicity, we will refer to $F(t, \vartheta_m^*)$ as the right-hand side of Eq. (5). This results in:

$$\vartheta_m^*(t_i) = \vartheta_m^*(t_{i-1}) + \frac{\delta t}{2}\left[F\left(t_i, \vartheta_m^*(t_i)\right) + F\left(t_{i-1}, \vartheta_m^*(t_{i-1})\right)\right], \tag{6}$$

where $\delta t = t_{i-1} - t_i$ represents the simulation time step. The Eq. (6) is non-linear with respect to $\vartheta_m^*(t_i)$ and is solved for each time step by a fixed-point iteration. The forward Euler method, which approximates the integral by the area of a rectangle, is used as the initial value for this iteration.

$$\vartheta_m^*(t_i) = \vartheta_m^*(t_{i-1}) + \delta t\ F\left(t_{i-1}, \vartheta_m^*(t_{i-1})\right). \tag{7}$$

The numerical accuracy of the trapezoidal rule method is directly influenced by the chosen simulation time step. In general, the numerical error decreases with decreasing simulation time step. Higher values of the simulation time step can lead to convergence problems in the regression algorithm, as shown in [19]. In the present work, the simulation time step is decoupled from the data averaging time. This solves the aforementioned convergence problems and allows to reduce the numerical error simply by choosing a simulation time step smaller than the data averaging time of the experimental data. However, the numerical method still requires input variable values at each simulation time step. Consequently, when the simulation time step is smaller than the data averaging time ($\delta t < \Delta t$), the input variables are linearly interpolated. The effects of varying these parameters or using an alternative numerical resolution method are explored in the Section 4.

The numerical solution of the differential equation requires the regression algorithm to be nonlinear. The combination of these factors makes the implementation of this procedure more challenging than the MLR procedure. In this context, there are some precedents for the implementation of this parameter identification procedure for low-temperature collectors [14, 20]. However, all of these implementations rely on closed-source, paid tools, which further complicates reproducibility. Furthermore, these works only demonstrate the implementation of the method for flat plate collectors. While the procedure is theoretically applicable to other types of technologies, similar to MLR, this generalization has not yet been demonstrated nor tested. As mentioned in the introduction, this work aims to further demonstrate the generality of the procedure and improve its reproducibility by providing well-described computational code (see the Data and Software Availability section). This code represents an improvement and continuation of the software provided in [5, 19].

3. Test facilities and experimental data

This section describes the test facilities, the collector tested, and the measurements used to determine the collector parameters.

3.1. Testing facilities and evaluated collectors

The experiments were carried out at the Solar Heater Test Bench (Banco de Ensayos de Calentadores Solares - BECS) located at the Solar Energy Laboratory (Laboratorio de Energía Solar - LES, http://les.edu.uy/) of the University of the Republic (Udelar) in Salto, Uruguay (latitude=$-31.28°$°S, longitude=$-57.92°$°W). This test facility, adapted by researchers at LES, is based on existing facilities at the National Renewable Energy Center (Centro Nacional de Energías Renovables - CENER) in Spain and is described in detail in [4]. It is noteworthy that in 2019 this test facility participated in a laboratory intercomparison at the Latin American regional level, organized by the PTB (Physikalisch-Technische Bundesanstalt), the German metrology institute. It received the highest rating in most of the test variables and received only two minor observations related to the determination of secondary variables, both of which have already been addressed by the laboratory [21].

For this study, the thermal performance of two solar thermal collectors was evaluated: a flat plate collector, denoted as FPC, and an evacuated tube collector with heat pipes, denoted as ETC-HP. The FPC, which serves as the reference collector in the aforementioned interlaboratory comparison, has a gross area of $2.02\,\mathrm{m}^2$ and is made of a copper plate and a selective titanium oxide coating, which contribute to its excellent thermal performance. The ETC-HP has a gross area of $1.55\,\mathrm{m}^2$ and consists of 10 evacuated tubes, each with an outside diameter of 59 mm and a length of 1.80 cm, spaced 18 mm apart. This collector is equipped with heat pipes measuring 168.7 cm in length, with 163 cm as the evaporator section and 5.7 cm as the condenser section. The diameters of the evaporator and condenser are 14 mm and 8 mm, respectively.

The FPC was tested from April 30 to May 15, 2021, and the ETC-HP was tested from September 3 to September 30, 2022. Both collectors were mounted on a mobile tracker with a manually adjustable horizontal tilt and an azimuth that could be adjusted either manually or automatically at 2-minute intervals.

3.2. Data set description

The tests were conducted in accordance with the ISO 9806:2017 standard. Throughout the experiments, a spatial average wind speed of 3 m/s was maintained using blowers. In addition, the flow rates were set to 2.40 L/min for the FPC and 1.90 L/min for the ETC-HP, following the standard recommendation. Five different measurement sequences were obtained for the FPC and six different sequences for the ETC-HP (due to its complex IAM) using the QDT method. The main characteristics of these measurement sequences for each collector are summarized in Table 1.

Table 1: Description of the measurement sequences performed on each collector for the QDT method.

Collector	Sec.	Date	Hour	ϑ_i (°C)	q (L/min)	$\vartheta_m - \vartheta_a$ (°C)	f_d	θ (°)	θ_L (°)	θ_T (°)
FPC	1a	04/30/2021	08:15-17:35	20.1(0.55)	2.388(0.89)	7.3	0.08-0.35	0-69	-	-
	2a	11/05/2021	09:35-12:45	16.1(0.17)	2.388(1.87)	3.5	0.06-0.95	0-44	-	-
	3a	08/05/2021	12:45-15:55	42.5(0.13)	2.388(1.01)	26.9	0.07-0.09	0-44	-	-
	3b	12/05/2021	12:45-15:55	61.8(0.10)	2.391(1.04)	45.9	0.07-0.11	0-44	-	-
	4a	15/05/2021	09:35-12:55	82.9(0.25)	2.389(0.83)	67.1	0.08-0.09	0-44	-	-
ETC-HP	1a	07/09/2022	07:51-17:15	22.9(0.49)	1.889(0.56)	3.0	0.12-0.26	-	0-8	0-72
	1b	27/09/2022	08:05-17:15	24.9(0.20)	1.892(0.62)	2.6	0.10-0.13	-	0-40	0
	2a	30/09/2022	11:15-14:30	23.0(0.16)	1.892(0.52)	2.5	0.17-0.99	-	0-18	0
	3a	04/09/2022	12:35-15:50	45.9(0.11)	1.892(0.28)	29.0	0.10-0.10	-	0-12	0
	3b	05/09/2022	12:35-15:50	66.9(0.17)	1.891(0.46)	47.0	0.09-0.10	-	0-12	0
	4a	03/09/2022	12:35-15:50	88.5(0.15)	1.892(0.77)	72.4	0.09-0.09	-	0-12	0

The table contains information about the test date, inlet temperature ϑ_i (mean and maximum variability), flow rate q (mean and maximum variability), mean temperature difference $\vartheta_m - \vartheta_a$, diffuse fraction

$f_d = G_{dh}/G_h$ (range of variation), angle of incidence and transverse and longitudinal angles of incidence (range of variation). All sequences meet the collector inlet temperature and flow stability requirements of the standard for the QDT method; variability is less than $\pm 1\,°C$ and $2\,\%$ of the mean, respectively.

The SST method used the same data set, but underwent different processing procedures to identify the subsequences or data points that met the specific measurement requirements of that method.

4. Results

In this section, we present and discuss the results of the two test methods, SST and QDT, as well as the two parameter identification procedures for the QDT method: MLR and DPI, both with the non-linear optimization method. Subsection 4.1 validates the DPI algorithm presented in this work and provides an analysis of the discrepancies between these test methods, especially for ETC-HP. In the following subsection (Subsection 4.2), we show the advantages of the DPI procedure over MLR, demonstrating its superiority for solar collector testing.

4.1. DPI algorithm validation

Table 2 shows the values of the parameters of the thermal models described in Eq. (1) for each test method, together with the typical P67 uncertainty of the parameters. For all the parameters, a t-statistic greater than 3 (ratio between the parameter value and its uncertainty) was obtained, indicating statistical significance, except for the parameter a_2, which had to be kept constant at zero in some cases, in accordance with the test standard. Node values for the IAM are reported at 10 degree intervals, where $K_b(80°)$ for FPC and $K_{bL}(\theta_L > 40°)$ and $K_{bT}(80°)$ for ETC-HP correspond to interpolated data, as is usually done for these high angle values.

For the QDT method and both parameter identification procedures, parameters were determined at four different data averaging times: 30 seconds, 1, 5, and 10 minutes. In the case of the MLR method, 5-minute averages were used for FPC and 10-minute averages were used for ETC-HP. This choice of data averaging time minimizes the deviation from the results obtained with the SST method, as demonstrated in previous studies [5, 8]. For the DPI procedure, although there are minimal changes in parameters with different data averaging times (as shown in the following subsection), we have found that the 30-second average provides the best option. In addition, a simulation time step of 30 seconds was chosen for the numerical simulation in the DPI algorithm.

The results of the SST and QDT-MLR have been previously presented and discussed in [5, 8] for FPC and ETC, respectively. The only difference in this study is the use of different test data for FPC. Considering the previous testing of this type of collector [7], both test methods have a relatively high degree of agreement. The main differences occurred in the parameters a_5, K_d for both collectors and in the parameter $K_b(\theta \geq 70°)$ for ETC-HP.

Table 2: Parameter values and uncertainty for each collector obtained using the different test methods and parameter identification procedures. Data not applicable is indicated by N/A.

Collector	FPC						ETC-HP					
Testing method	SST (10 minutes)		QDT-MLR (5 minutes)		QDT-DPI (30 second)		SST (10 minutes)		QDT-MLR (10 minutes)		QDT-DPI (30 second)	
Parameters	Value	Uncer.	Value	Uncer.	Value	Uncer.	Value	Uncer.	Value	Uncer.	Value	Uncer.
$\eta_{0,b}$	0.726	N/A	0.718	$\pm$0.0018	0.72	$\pm$0.0009	0.371	N/A	0.367	$\pm$0.0027	0.365	$\pm$0.0003
K_d	0.905	N/A	0.973	$\pm$0.005	0.941	$\pm$0.004	1.007	N/A	1.181	$\pm$0.033	1.237	$\pm$0.003
a_1	4.499	$\pm$0.0186	4.311	$\pm$0.041	4.331	$\pm$0.02	1.682	$\pm$0.06	1.686	$\pm$0.044	1.677	$\pm$0.004
a_2	0	N/A	0.001	$\pm$0.0006	0.001	$\pm$0.0003	0	N/A	0	N/A	0	N/A
$a_5 \times 1000$	11.0	$\pm$0.6	11.4	$\pm$0.3	12.7	$\pm$0.2	207.6	$\pm$1	126	$\pm$4	168	$\pm$0.7
θ	K_b		K_b		K_b		K_{bL}	K_{bT}	K_{bL}	K_{bT}	K_{bL}	K_{bT}
0	1		1		1		1	1	1	1	1	1
10	1.00		0.99		0.99		0.99	1.01	0.98	1.01	0.98	1.00
20	1.00		0.99		0.99		0.99	1.07	1.00	1.07	1.00	1.09
30	1.00		0.99		0.98		1.00	1.15	1.00	1.20	1.00	1.18
40	1.00		0.98		0.98		0.97	1.29	0.93	1.39	1.00	1.36
50	0.97		0.94		0.94		0.77	1.40	0.74	1.58	0.80	1.57
60	0.90		0.86		0.87		0.58	1.44	0.56	1.57	0.60	1.56
70	0.72		0.74		0.68		0.39	1.18	0.37	1.68	0.40	1.75
80	0.36		0.37		0.34		0.19	0.59	0.19	0.84	0.20	0.88
90	0		0		0		0	0	0	0	0	0

In the case of QDT-DPI, the results of both collectors show small differences compared to QDT-MLR. Again, the largest differences are observed in the parameters a_5, K_d and $K_b(\theta \geq 70°)$, but the discrepancies are smaller than those observed in SST vs. QDT-MLR. Regarding the differences observed in the parameters K_d and $K_b(\theta \geq 70°)$, it does not seem to be a clear trend that one algorithm gives better results than the other. The same applies to a_5 for the FPC collector. However, in the case of a_5 for the ETC-HP collector, the DPI algorithm gives values closer to those of the SST method, suggesting a better modeling of the transient effects of the collectors.

It is important to note that the determination of the a_5 value by the SST method follows the procedure described in section 25.2 of the ISO 9806:2017 standard. This involves operating the covered collector in a steady state, uncovering it and waiting for it to reach a new steady state. The a_5 value is obtained by integrating the thermodynamic model between these two operating points. However, taking into account the mass and specific heat of ETC-HP materials, according to section 25.4 of the ISO 9806:2017, a_5 values of $5459\,\mathrm{J/°Cm^2}$ were obtained, which are significantly lower than the previous SST and QDT values in Table 2.

One interpretation of this difference could be that the procedure in section 25.4 of the ISO 9806:2017 does not take into account the phase change within the heat pipe. This oversight may slow down the temperature changes at the collector outlet, resulting in an effective thermal capacity greater than predicted by this method (section 24.5 of the ISO 9806:2017). In other words, a_5 from QDT and SST takes these effects into account, resulting in lower values for this parameter. It is imperative to deepen this analysis and the interpretation of the a_5 parameter for this type of collector, which represents future work.

Despite the observations mentioned in the previous paragraph, we conclude that the DPI algorithm presented in this paper has been successfully validated for both collectors and provides equivalent results to SST and QDT-MLR. Although MLR and DPI give equivalent results when their optimal data averaging time is considered, the latter has some advantages that are discussed in the following subsection.

4.2. Superiority of the DPI procedure

This subsection shows the advantages of the DPI procedure over the MLR. Subsection 4.2.1 shows the robustness of DPI with respect to data averaging time, which results in lower parameter variability, and also presents its ability to provide more accurate estimates of useful power and the consequent reduction in parameter uncertainty. Subsection 4.2.2 shows that the DPI procedure yields more reliable IAM results, showing greater robustness to experimental data and the possibility of reducing test duration.

4.2.1. Robustness against data averaging time

In this subsection, the robustness of the parameter identification procedures with respect to the data averaging time is evaluated. For this comparison, parameter values for both collectors were determined using the QDT method with different averaging times: 30 seconds, 1, 5 and 10 minutes. While 30 seconds is the value suggested by the standard, 1 and 10 minutes are the typical values used in the literature. The 1 minute time base was chosen as an intermediate value between 30 seconds and 5 minutes, which also reduces the number of samples to be treated computationally. Both MLR and DPI procedures were used for parameter identification. The results are summarized in Table 3. For each parameter, the mean value and the maximum variability are presented, taking into account the different data averaging times mentioned above. The maximum variability for each parameter was calculated as the difference between the maximum and minimum values and then expressed as a percentage of the average. At the end of the table, the average of the maximum variability for all parameters is shown. For simplicity, the table presents the a_{50} factor instead of a_1 and a_2, as it represents the overall thermal loss factor at a temperature difference of 50 K. This factor is calculated as $a_{50} = a_1 + 50 \times a_2$. Additionally, the K_b values at 0° and 90° are omitted since they are fixed by physical constraints.

In most cases, the average values of the parameters show small differences with respect to the optimal values of the table Table 2, so the parameter specification procedures differ mainly in the maximum

Table 3: Average values and maximum variability of the parameters for each collector obtained by the QDT method and each parameter identification procedure, MLR and DPI, taking into account different data averaging times: 30 seconds, 1, 5 and 10 minutes.

Collector	FPC				ETC-HP							
Method	QDT-MLR		QDT-DPI		QDT-MLR				QDT-DPI			
Parameters	Ave.	Var.	Ave.	Var.	Ave.		Var.		Ave.		Var.	
$\eta_{0,b}$	0.718	0.8 %	0.719	0.4 %	0.358		5.3 %		0.365		0.3 %	
K_d	0.969	6.8 %	0.965	3.5 %	1.352		26 %		1.234		2.3 %	
a_{50}	4.359	1.6 %	4.385	0.9 %	1.549		16 %		1.659		6.0 %	
$a_5 \times 1000$	9.9	42.4 %	11.7	14.5 %	62.6		196 %		163		8.0 %	
θ	K_b	K_b	K_b	K_b	K_{bL}	K_{bT}	K_{bL}	K_{bT}	K_{bL}	K_{bT}	K_{bL}	K_{bT}
10	0.99	1.0 %	0.99	0.0 %	0.96	1.03	5.2 %	3.9 %	0.98	1.00	0.0 %	1.0 %
20	0.99	0.0 %	0.99	0.0 %	0.91	1.10	22 %	5.4 %	1.00	1.09	0.0 %	0.0 %
30	0.99	0.0 %	0.99	1.0 %	1.00	1.21	0.0 %	0.8 %	1.00	1.18	0.0 %	0.0 %
40	0.98	0.0 %	0.98	0.0 %	0.98	1.39	7.1 %	0.7 %	1.00	1.36	0.0 %	0.0 %
50	0.94	4.3 %	0.94	0.0 %	0.79	1.56	7.6 %	2.6 %	0.80	1.57	0.0 %	0.6 %
60	0.86	1.2 %	0.87	1.2 %	0.59	1.59	6.8 %	1.9 %	0.60	1.56	0.0 %	0.6 %
70	0.73	6.8 %	0.70	5.7 %	0.39	1.55	7.6 %	13 %	0.40	1.77	0.0 %	4.5 %
80	0.37	5.4 %	0.35	5.7 %	0.20	0.78	5.1 %	13 %	0.20	0.89	0.0 %	4.5 %
Var. all	-	5.9 %	-	2.8 %	-		17.2 %		-		1.6 %	

variability.

Regarding the MLR procedure, the results show a considerable variability with respect to the data averaging time, which is in line with previous findings [14] for FPC. This variability is particularly pronounced in the case of the ETC-HP, with many parameters showing values greater than 10 %. To obtain accurate parameter values, a data averaging time equal to or greater than 5 minutes (approximately) is required. However, the specific data averaging time that gives the best results, closest to the SST parameter values, depends on the collector technology. Consequently, this variable (data averaging time) must be set specifically for each collector type, which is a clear disadvantage of this procedure. The optimal data averaging time has been found in previous studies [5, 22] and corresponds to 5 minutes and 10 minutes for FPC and ETC-HP, respectively.

To further understand and clarify the above results, the mean squared error of the useful power was also calculated for each case and the results are shown in Figure 1. This error is expressed as a percentage of the average useful power for each collector, being $504\,\mathrm{W/m^2}$ and $326\,\mathrm{W/m^2}$ for FPC and ETC respectively. This figure shows a clear trend: the mean squared power error for the MLR procedure decreases with data averaging time. This trend illustrates why it is necessary to work with relatively long averaging times in the case of the MLR procedure; this procedure has difficulty modeling the transient effects of the collectors at low data averaging times, resulting in high errors. One explanation for this is that since $d\vartheta_m/dt$ is estimated using finite differences, i.e. $d\vartheta_m/dt \approx \Delta\vartheta_m/\Delta t$, the relative error in this variable is inversely proportional to the experimental temperature differences $\Delta\vartheta_m$ [22]. At low data averaging times, the differences $\Delta\vartheta_m$ are small and therefore the relative error of the associated independent variable is high, which naturally introduces error into the modeling and explains the behavior shown in Figure 1.

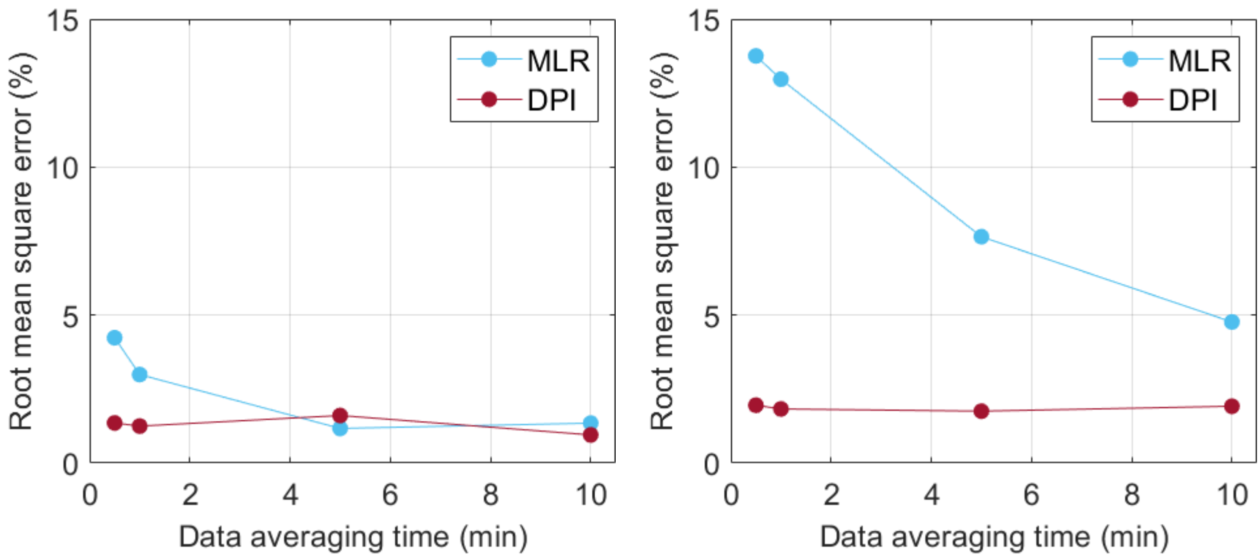

(a) FPC. (b) ETC.

Figure 1: Root mean square error of useful power as a function of data averaging time for both collectors and parameter identification procedures of the QDT methodology. This error is expressed as a percentage of the average useful power for each collector, which is 504 W/m^2 and 326 W/m^2 for FPC and ETC, respectively.

The DPI procedure, Table 3, also shows a significant reduction in parameter variability compared to the MLR procedure. In particular, this behavior is accentuated in the case of the ETC-HP collector, with a reduction in the variability of almost all the parameters. This makes the method less dependent on data averaging time and more robust than the MLR procedure. Figure 1 shows a clear trend for the DPI procedure that, in contrast to the MLR procedure, the mean squared error is approximately constant and independent of the data averaging time.

In addition, Figure 1 allows a depth comparison between MLR and DPI. In the case of the FPC collector, it can be seen that the MLR and DPI procedures have similar errors for data averaging times greater than 5 minutes. However, for data averaging times less than or equal to 1 minute, the DPI procedure provides more accurate estimates, i.e., the root mean square error is lower. In the case of the ETC collector, the DPI procedure provides more accurate estimates over the entire range of data averaging times analyzed. In conclusion, the superiority of the DPI procedure over the MLR method is particularly evident at low averaging times (30 seconds and 1 minute) for both FPC and ETC.

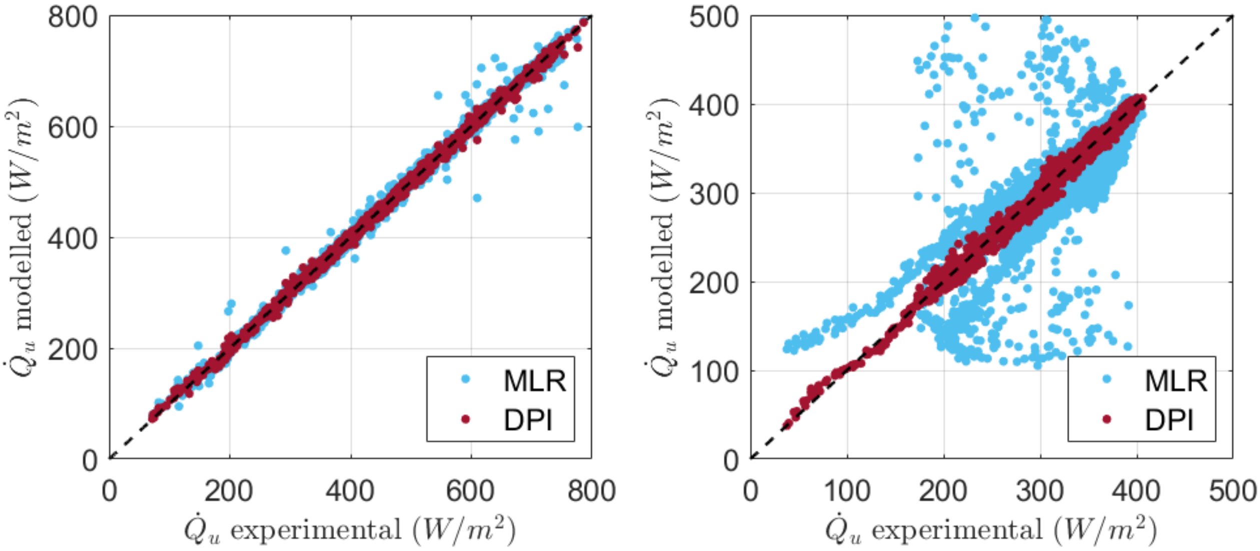

(a) FPC. (b) ETC.

Figure 2: Scatter plots of useful power for both collectors and parameter identification procedures of the QDT method. Data correspond to 30 seconds of data averaging.

Complementing the previous paragraph, Figure 2 shows the scatter plots of the useful power for each collector and parameter identification method for a data averaging time of 30 seconds. This figure further highlights the fact that the DPI procedure has a lower mean square error, as shown by the lower dispersion of these figures. In particular, for the ETC-HP collector, these differences are more pronounced, clearly showing the advantages of the DPI procedure for this specific technology. Consequently, for this collector, the parameter uncertainty estimated by the DPI procedure at this data averaging time is an order of magnitude lower than that estimated by the MLR method at its optimal data averaging time (10 minutes), as shown in Table 2.

It is important to note that although the study carried out in this section focuses on the effect of data averaging time on parameter values, this variable also affects the assessment of experimental data quality, i.e. the verification of compliance with the requirements of the standard. Some measured variables, in particular wind speed, vary significantly with averaging time, potentially complying with the standard in some cases but not in others. As the collectors in this work are covered, wind speed does not play a significant role in the thermal modeling and power output. Although there can be minor deviations from the wind speed requirements in the analysis, they do not significantly affect the results. However, this should be investigated in more detail when applying the DPI tool to uncovered collectors, which represents future work.

4.2.2. Improving the reliability of IAM estimation

In this subsection it is shown that the DPI procedure yields more reliable IAM results, especially for the ETC-HP technology, overcoming one of the main drawbacks of the MLR procedure. This is due to its improved transient modeling, which provides robustness to experimental data. Specifically, we evaluate the feasibility of using data sequences for day type 1 that are not symmetric with respect to solar noon, which is a requirement of the standard that results in higher testing times. Thus, the elimination of this requirement allows for a reduction in test times by shortening the measurement sequences associated with day type 1.

To achieve this, each day type 1 measurement sequence from Table 1 was split into two segments, distinguishing whether the data were taken before or after solar noon. Separate training datasets were then created sharing the day type 2, 3, and 4 sequences, but being difference in the previously generated day type 1 sub-sequences. Two different datasets were created for the FPC collector and four for the ETC-HP collector. The next step was to identify the parameter values of the collectors using the different data sets. In each case, the optimal data averaging time was used for each collector and parameter identification procedure. After parameter identification, the average of each parameter was calculated based on the results obtained from the different data sets. The maximum variability for each parameter was calculated as the difference between the maximum and minimum values and then expressed as a percentage of the average parameter value. The results of this analysis for each collector and parameter identification procedure are presented in Table 4. At the end of the table, the average of the maximum variability for all tests are shown, considering all parameters and the K_b values.

In the case of the FPC collector, it is observed that the average values of the parameters are close to the optimal values in Table 2, and the maximum variability is relatively small in both cases, MLR and DPI, being slightly lower in the case of DPI. Therefore, for this particular type of collector, it is possible to use measurement sequences for day type 1 that are not symmetrical with respect to solar noon in both cases (MLR and DPI). However, it is noted than the DPI provide better results, specially for the a_5 parameter and the K_b values for the higher incident angles.

On the other hand, a different behavior is observed in the case of the ETC-HP collector. In the case of the MLR procedure, it is observed that the average values of some parameters differ from their optimal values, but the differences are small. This is particularly the case for the IAM values for large angles of incidence. In addition to these differences, a significant maximum variability is also observed, reaching up to 18 % in some cases. For this reason, it is not advisable to use asymmetric measurements for day type 1 in the MLR procedure. On the contrary, in the case of the DPI procedure, it is observed that the average values of the parameters are close to the optimal values and the maximum variability is relatively small. Therefore, in the case of DPI, it is possible to use asymmetric measurements for day type 1. This makes DPI a more versatile and reliable method, since its results do not depend on the type of collector.

Table 4: Average values and maximum variability of the parameters for each collector obtained by the QDT method and by each parameter identification procedure, MLR and DPI, considering different data sets.

Collector	FPC				ETC-HP							
Method	QDT-MLR		QDT-DPI		QDT-MLR				QDT-DPI			
Parameters	Ave.	Var.	Ave.	Var.	Ave.		Var.		Ave.		Var.	
$\eta_{0,b}$	0.719	0.1 %	0.721	0.0 %	0.365		1.4 %		0.363		0.6 %	
K_d	0.971	0.0 %	0.938	0.0 %	1.202		2.6 %		1.251		1.4 %	
a_{50}	4.418	0.1 %	4.404	0.1 %	1.621		5.3 %		1.637		2.2 %	
$a_5 \times 1000$	11.7	2.6 %	13.0	0.8 %	122		9.1 %		161		8.7 %	
θ	K_b	K_b	K_b	K_b	K_{bL}	K_{bT}	K_{bL}	K_{bT}	K_{bL}	K_{bT}	K_{bL}	K_{bT}
10	0.99	0.0 %	0.99	0.0 %	0.97	1.03	0.0 %	0.0 %	1.00	1.01	0.0 %	1.0 %
20	0.99	0.0 %	0.99	0.0 %	0.99	1.08	0.0 %	4.9 %	0.98	1.09	0.0 %	0.9 %
30	0.99	0.0 %	0.99	0.0 %	1.00	1.21	1.0 %	3.7 %	1.00	1.19	0.0 %	0.8 %
40	0.99	1.0 %	0.98	0.0 %	0.93	1.40	0.0 %	9.9 %	1.00	1.37	0.0 %	0.7 %
50	0.95	1.1 %	0.95	0.0 %	0.75	1.59	15 %	6.4 %	0.80	1.57	0.0 %	1.9 %
60	0.86	3.5 %	0.87	3.5 %	0.56	1.57	15 %	7 %	0.60	1.55	0.0 %	7.1 %
70	0.65	22 %	0.63	13 %	0.37	1.66	16 %	18 %	0.40	1.74	0.0 %	6.3 %
80	0.33	22 %	0.32	16 %	0.19	0.83	16 %	10 %	0.20	0.87	0.0 %	6.9 %
Var. all	-	4.3 %	-	2.7 %	-		8.4 %		-		1.7 %	
Var. K_b	-	6.1 %	-	4.0 %	-		9.3 %		-		1.6 %	

It should be noted that although the data corresponding to day type 1 are mostly clear skies and could in principle be considered quasi-stationary, significant variations in IAM and solar irradiance levels occur near sunrise and sunset, causing significant transients in the collectors. For this reason, the standard requires that the measurement sequences associated with this type of day be symmetrical with respect to solar noon; this compensates for these effects and improves the reliability of the results, but at the cost of longer test times. The removal of this requirement increases the demands on the parameter identification procedure, and the accurate identification of the IAM for high angles of incidence will depend on the approach used to deal with such transients. In this regard, the results obtained in this section are due to the fact that the DPI procedure has a better ability to model transient effects than the MLR procedure.

Finally, it is important to note that in all cases (collectors and averaging times), a simulation time step of 30 seconds was used for the numerical simulation in the DPI algorithm. Since this variable must be specified by the tester, different values were studied to evaluate its impact on the results. This analysis demonstrated that the results and conclusions presented in this paper remain consistent as long as the interval is kept below 1 minute. Reducing the interval below 30 seconds did not significantly improve parameter estimation but did slow down program execution. Therefore, a simulation time step of 30 seconds is recommended, as it proved suitable for both collectors, ensuring modeling accuracy compared to MLR while maintaining efficient program execution. Additionally, different numerical solution algorithms for the differential equations (e.g., forward Euler, backward Euler, multipass methods) and various interpolation schemes for the experimental data were tested, with no significant differences observed in the results.

5. Conclusions

In this work, a DPI procedure has been presented for QDT testing of low temperature glazed solar collectors. The algorithm's results were compared with the SST and QDT-MLR methods using two solar collectors of this type: an FPC and an ETC-HP. This work represents the first precedent of the implementation of the DPI procedure for the ETC collector. By comparison with the SST reference, the proposed DPI procedure was validated. This work represents progress in demonstrating the generality of the general procedure, that is, its applicability to different collector technologies.

Although the MLR and DPI procedures provided similar parameter values for their optimal data averaging times, the latter procedure was demonstrated in this work to have significant advantages in terms of reliability of results. In this regard, a sensitivity analysis of the data averaging time was performed, which revealed the large variability of the results of the MLR procedure, especially in the case of the ETC-HP collectors. This highlights the particular challenges of the MLR procedure for this type of collector. It also shows the need for this procedure to work with data averaging times longer than 5 minutes to ensure the reliability of the results, which is in line with previous work. For averaging times less than 5 minutes, the root mean square error of the useful power increases significantly, introducing uncertainty in the process and in the final parameter values. The specific data averaging time that gives the best results, closest to the SST parameter values, but depends on the collector technology.

In contrast, the DPI procedure shows much lower variability with respect to data averaging time, and the mean square error of the useful power remains stable over a wide range of data averaging times considered. The greatest reduction in parameter variability and mean square error is observed in the case of the ETC-HP, indicating that DPI is a better option for this particular technology. The fact that the characteristic parameter values do not depend on the averaging time makes the DPI procedure more robust. However, we recommend using averaging times for the DPI procedure that are less than or equal to 1 minute; this ensures the advantages of this method over the MLR for both types of collectors in terms of precision of useful power estimates and reduction of parameter uncertainty.

Another advantage of the DPI procedure that has been demonstrated is that it provides more reliable results for the IAM, especially with respect to the nodal values of this function at high angles of incidence. In addition, the DPI procedure was demonstrated to enable the use of asymmetric measurement sequences with respect to solar noon for day type 1, which is currently required by the test regulations. Removing this requirement from the standard would allow for reduced test times by shortening the measurement sequences dedicated to Day Type 1. This also suggests that the DPI procedure is a better alternative for testing collectors with asymmetric IAM, i.e. collectors whose IAM is not symmetrical with respect to the longitudinal and/or transverse plane.

A drawback of DPI procedures is that their implementation requires more complex mathematical tools. Although some literature describes implementations of this procedure, they are often based on closed code or paid programs, which pose challenges for replication. To address this limitation, a freely available and documented computational code is provided to facilitate the replication of this work and to broaden the application of the DPI procedure across different testing laboratories worldwide.

Acknowledgments

The authors would like to thank the Ministerio de Industria, Energía y Minería (MIEM, Uruguay), especially its Dirección Nacional de Energía (DNE), the Fideicomiso Uruguayo de Ahorro y Eficiencia Energética (Fudaee, Uruguay) and the Corporación Nacional para el Desarrollo (CND, Uruguay), for having provided financial and logistical support for the development of the BECS facility and for having promoted this project with local capacities. The authors are also grateful to the PTB of Germany for promoting and financing the inter-laboratory on efficiency test of solar collectors, which has given us technical certainty about our local testing capabilities. The authors acknowledges financial support from the CSIC Group's Program, Universidad de la República, Uruguay.

Appendix A. Data and software availability

To facilitate the reproduction of DPI procedure tests for FPC and ETC collectors, a Matlab program implementing this algorithm is provided and can be downloaded: http://les.edu.uy/RDpub/PITool_STCT_v2-program.rar. This program is intended for general use with low-temperature collectors with covers, with uniaxial or biaxial IAM, and represents a second version of the program provided in [5]. The program calculates and reports the values of the characteristic parameters, together with their uncertainties and t-statistics (the ratio between the parameter value and its uncertainty). For the parameter a_2, it is possible to set arbitrary upper and lower limits, so that the parameter can be set to zero if a positive value is obtained with a t-statistic less than 3 (in this case, both limits must be set to zero). Note, however, that the program does not check the quality of the experimental data set or its compliance with the requirements of the ISO 9806:2017 standard, which should be ensured by the practitioner before using it. However, it does provide the recommended graphs to assess the variability of the data set. The software is provided with the two experimental data sets used in this work.

References

[1] ISO-9806, Solar energy – solar thermal collectors – test methods, Standard, International Organization of Standarization, Switzerland (2017).

[2] ASHRAE-93, Methods of testing to determine the thermal performance of solar collectors, Standard, American Society of Heating, Refrigerating and Air-Conditioning Engineers, USA (2014).

[3] D. Rojas, J. Beermann, S. Klein, D. Reindl, Thermal performance testing of flat-plate collectors, Solar Energy 82 (8) (2008) 746 – 757. doi:https://doi.org/10.1016/j.solener.2008.02.001.

[4] J. M. Rodríguez-Muñoz, I. Bove, R. Alonso-Suárez, Novel incident angle modifier model for quasi-dynamic testing of flat plate solar thermal collectors, Solar Energy 224 (2021) 112–124. doi:https://doi.org/10.1016/j.solener.2021.05.026.

[5] J. M. Rodríguez-Muñoz, I. Bove, R. Alonso-Suárez, Improving the experimental estimation of the incident angle modifier of evacuated tube solar collectors with heat pipes, Renewable Energy 235 (2024) 121240. doi:https://doi.org/10.1016/j.renene.2024.121240.
URL https://www.sciencedirect.com/science/article/pii/S0960148124013089

[6] S. Fischer, W. Heidemann, H. Müller-Steinhagen, B. Perers, P. Bergquist, B. Hellström, Collector test method under quasi-dynamic conditions according to the european standard en 12975-2, Solar Energy 76 (1) (2004) 117 – 123. doi:https://doi.org/10.1016/j.solener.2003.07.021.

[7] T. Osório, M. J. Carvalho, Testing of solar thermal collectors under transient conditions, Solar Energy 104 (2014) 71 – 81, solar heating and cooling. doi:https://doi.org/10.1016/j.solener.2014.01.048.

[8] J. M. Rodríguez-Muñoz, A. Monetta, I. Bove, R. Alonso-Suárez, Ensayo cuasi-dinámico de colectores solares de placa plana en uruguay de acuerdo a la norma iso 9806:2017, ENERLAC. Revista de energía de Latinoamérica y el Caribe 4 (2) (2020) 10–26.

[9] J. Muschaweck, W. Spirkl, Dynamic solar collector performance testing, Solar Energy Materials and Solar Cells 30 (2) (1993) 95 – 105. doi:https://doi.org/10.1016/0927-0248(93)90011-Q.

[10] M. Bosanac, A. Brunotte, W. Spirkl, R. Sizmann, The use of parameter identification for flat-plate collector testing under non-stationary conditions, Renewable Energy 4 (2) (1994) 217–222.

[11] S. Fischer, W. Heidemann, H. Müller-Steinhagen, B. Perers, Collector parameter identification-iterative methods versus multiple linear regression, in: ISES Solar World Congress, International Solar Energy Society (ISES,, 2003, pp. 14–19.

[12] N. Janotte, S. Meiser, D. Krüger, E. Lüpfert, R. Pitz-Paal, S. Fischer, H. Müller-Steinhagen, Quasi-dynamic analysis of thermal performance of parabolic trough collectors, in: SolarPACES 2009 Conference Proceedings, 2009.

[13] A. Hofer, D. Büchner, K. Kramer, S. Fahr, A. Heimsath, W. Platzer, S. Scholl, Comparison of two different (quasi-) dynamic testing methods for the performance evaluation of a linear fresnel process heat collector, Energy Procedia 69 (2015) 84–95, international Conference on Concentrating Solar Power and Chemical Energy Systems, SolarPACES 2014. doi:https://doi.org/10.1016/j.egypro.2015.03.011.

[14] S. Fahr, U. Gumbel, A. Zirkel-Hofer, K. Kramer, In situ characterization of thermal collectors in field installations, in: Proceedings of EuroSun, 2018. doi:0.18086/eurosun2018.12.01.

[15] QAiST, Performance testing of evacuated tubular collectors, Report, Quality Assurance in Solar heating and cooling Technology (2012).

[16] W. R. McIntire, Factored approximations for biaxial incident angle modifiers, Solar Energy 29 (4) (1982) 315 – 322. doi:https://doi.org/10.1016/0038-092X(82)90246-8.

[17] D. Bertsekas, Nonlinear Programming, Athena Scientific, 1999.

[18] B. Perers, An improved dynamic solar collector test method for determination of non-linear optical and thermal characteristics with multiple regression, Solar Energy 59 (4) (1997) 163 – 178. doi:https://doi.org/10.1016/S0038-092X(97)00147-3.

[19] J. M. Rodríguez-Muñoz, I. Bove, R. Alonso-Suárez., A detailed dynamic parameter identification procedure for quasi-dynamic testing of solar thermal collectors, in: Proceedings of Solar World Congress, 2021. doi:doi:10.18086/swc.2021.25.01.

[20] W. Spirkl, J. Muschaweck, P. Kronthaler, W. Scholkopf, J. Spehr, In situ characterization of solar flat plate collectors under intermittent operation, Solar Energy 61 (3) (1997) 147–152.

[21] S. Fischer, Quality infrastructure for energy efficiency and renewable energy in latin america and the caribbean, report # 95309, Report, Intituto Metrológico Aleman - PTB (2020).

[22] J. M. Rodríguez-Muñoz, Ensayos de desempeño térmico de colectores solares de placa plana, Thesis, Universidad de la República (Uruguay). Facultad de Ingeniería. (2021). doi:10.13140/RG.2.2.23050.18881.